Building a Ferromagnetic Resonance Setup

van Galen, J.T.

Award date:
2017

Eindhoven University of Technology

Bachelor end project

Building a Ferromagnetic Resonance Setup

J.T. van Galen

Supervised by

dr. M.H.D. Guimaraes

ir. J. Lucassen

Responsible lecturer

prof.dr.ir. H.J.M. Swagten

July, 2017

Abstract

The demand for computing speed and storage density is ever increasing. To sustain this exponential growth, spintronic based devices, which utilize the spin degree of freedom of an electron, have shown great promise [1]. Technologies such as STT-RAM and racetrack memory offer fast, non-volatile and energy efficient solutions for information storage. For the development of these techniques, new magnetic thin film materials are required that have a low damping or high anisotropy. The characterization of these magnetic properties is an important part of developing these new materials and can be time consuming depending on the method used. An often used technique for the characterization of the magnetic properties of a material is ferromagnetic resonance. In this project we assemble an easy-to-use ferromagnetic resonance setup that is able to measure the effective magnetization and damping in magnetic materials. Ferromagnetic resonance relies on the excitation of the magnetic moment of a material by a microwave magnetic field. This excitation will absorb the microwave power and from the absorption spectrum the magnetic properties can be derived. The setup makes use of field modulation, allowing for a differential measurement of the absorption spectrum, increasing the signal-to-noise ratio of the measurement. Tests on a permalloy sample have shown that measurements with the setup can be performed in a relatively short amount of time with high accuracy. The setup can thus be a useful for the characterization of new materials used in research on spintronic based technologies.

Contents

Chapter 1

Introduction

In recent years, the need for faster computing power and high density storage has increased exponentially. To sustain this growth a lot of research is done in the emerging field of spintronics, that makes use of the electron spin degree of freedom for data storage and transfer applications [1]. Promising new technologies like race track memory, MRAM and STT-RAM, offer fast, power efficient and high density storage solutions. To realize the development of these spintronic based devices, materials with specifically tuned magnetic properties are required.

Ferromagnetic materials are often used in research focussed on spintronics. Two essential properties of ferromagnetic materials are its anisotropy and damping. A high anisotropy is essential for the stabilization of magnetic domains. This can for example be useful in the implementation of racetrack memory, where data is stored in moving magnetic domains on a nanowire. The Gilbert damping of a material determines the relaxation of the magnetic moment towards equilibrium. It thus tells us how easy the magnetic moment in a material can transition between different states. A low Gilbert damping allows for easy and fast transitioning, thereby requiring little energy [2]. A low damping is thus essential for the development of fast and energy efficient spintronic devices.

A useful tool to characterize the effective magnetization and Gilbert damping is ferromagnetic resonance (FMR). In ferromagnetic resonance a ferromagnetic material is excited by a microwave ($\sim$GHz) signal leading to a precession of the magnetic moment around the equilibrium axis. For a specific combination of microwave frequency and magnetic field strength, the precession will resonate and absorb the power of the microwave signal. Measurement of the absorbed power results in a characteristic resonance peak and from the position and width of this resonance peak it is possible to accurately determine the anisotropy and damping of a material.

The goal of this project is to assemble and optimize an easy-to-use FMR setup, in which the sample is flipped upside down and placed on top of a waveguide. A microwave signal is send through the waveguide, which induces an Oersted field in the sample that exciting the precession of the magnetic moment. By measuring the output power of the waveguide, the power absorbed by the excitation can be determined. By making use of magnetic field modulation in combination with a lock-in amplifier, a high signal-to-noise ratio can be achieved by filtering out all noise and background that is not field dependent.

The group currently already has a VNA-FMR setup available that is able to do FMR measurements, but its measurements are noisier and it requires careful calibration of the phase of the signal to give accurate results. The setup that we build provides a faster and easier way of measuring the ferromagnetic resonance in magnetic materials and is thus a useful tool in the characterization of thin film magnetic materials used in research projects in the Physics of Nanostructures (FNA) group.

In chapter 2 we discuss the theory that explains what ferromagnetism is and how the magnetic properties of a material can determined by ferromagnetic resonance. In chapter 3 the design of the setup is discussed and it is explained how the setup operates. In chapter 4 we verify the working of the setup by measuring the ferromagnetic resonance in a permalloy thin film sample and determining its effective magnetization and damping. At last, in chapter 5 we evaluate working of the setup.

Chapter 2

Theory

In this chapter we will discuss the physics that are necessary to understand the principles of ferromagnetic resonance. First we discus what ferromagnetism is and how the magnetic moment of a ferromagnet behaves under the influence of a strong magnetic field. Followingly, we describe the dynamics of the magnetic moment after excitation with a weak microwave field. We discuss how this leads to ferromagnetic resonance and how this allows us to determine the anisotropy and damping in a magnetic material.

2.1 Ferromagnetism

2.1.1 Heisenberg model

A material is ferromagnetic when it has a permanent magnetic moment in the absence of an external magnetic field. The spontaneous magnetization arises from the interaction between the spins of neighboring electrons in a crystal lattice. A simple model of a ferromagnet is given by the Heisenberg model, which has the Hamiltonian:

$$\mathcal{H} = \frac{1}{2} \sum_{\substack{i,j \\ i \neq j}}^{n} J_{ij} \boldsymbol{S_i} \cdot \boldsymbol{S_j}, \tag{2.1}$$

where J_{ij} is the exchange constant and $\boldsymbol{S_i} \cdot \boldsymbol{S_j}$ the exchange interaction between the spin angular momenta of two neighboring electrons. The expectation value for the Heisenberg Hamiltonian is called the exchange energy E_{ex}. The ground state of the system is the state in which the exchange energy is minimal. For $J < 0$ this means that the energy is minimal when the spins align parallel to each other and for $J > 0$ the energy is minimal when the spins align anti-parallel to each other. These cases are called ferromagnetic order and anti-ferromagnetic order respectively. In the ferromagnetic case this results in a spontaneous magnetic moment in the bulk material. In the anti-ferromagnetic case, the neighboring spins align in opposite directions, resulting in no net magnetic moment.

As temperature increases, the thermal energy k_bT becomes comparable to the exchange energy. When $E_{ex} = k_bT_c$, where T_c is the Curie temperature, the thermal energy starts dominating the exchange energy and the spins align randomly, resulting in a loss of the spontaneous magnetization. Above the Curie temperature the material starts behaving like a paramagnet.

2.1.2 Ferromagnetic hysteresis

Below the Curie temperature the ferromagnet has a spontaneous magnetization and thus its behavior under the influence of a magnetic field is different than that of a paramagnet. When applying an external magnetic field to a ferromagnetic material, the spins in the material align in the direction of the field. The magnetization M of the material depends not only on the strength of the applied field, but also on its current alignment. All ferromagnets have a magnetic anisotropy, a dependence of the magnetic properties, based on the direction of the magnetic moment. Ferromagnets have a preferred direction of alignment called the easy axis. The anisotropy energy is given by

$$E_A = K \sin^2(\theta), \tag{2.2}$$

where K is the anisotropy constant and θ the angle between the magnetic field direction and easy axis. The anisotropy energy is minimal when $\theta = 0$, thus it is easier to align the magnetic moment with the easy axis in comparison to other directions. The hysteretic behavior of a ferromagnet with an external field in the direction of the easy axis, is shown in figure 2.1 as the solid line. For a strong magnetic field all spins in the ferromagnet are aligned in the direction of the field resulting in a saturation magnetization M_S. When the field is switched off, the magnetization of the material does not go back to zero, but a remnant magnetization M_r stays present. When the magnetic field is in the direction of the easy axis, the remnant magnetization is equal to the saturation magnetization. As the magnetic field is increased in the opposite direction of the magnetization, the magnetization does not immediately change direction as well. The strength of the field required to flip the magnetization in the opposite direction is called the coercive field H_C. As the coercive field is reached the magnetization flips direction. When the angle between the magnetic field and easy axis is nonzero, the ferromagnet shows a different behavior shown as the dashed line in figure 2.1. The hysteresis loop becomes narrower and the coercive field and remnant magnetization decrease. For use in for example hard drives or racetrack memory, the ferromagnetic material needs to show a high anisotropy and strong saturation magnetization for stabilization of the magnetic domains.

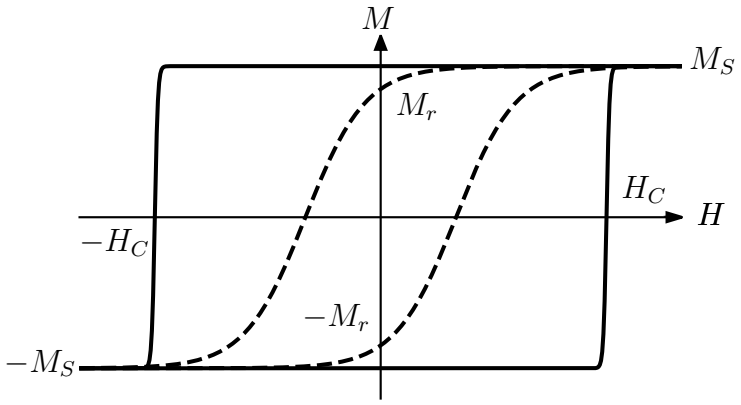

Figure 2.1: The magnetic moment of a ferromagnet shows hysteresis depending on the direction of the field sweep. For strong fields, the magnetization is saturated with strength M_S. The ferromagnet has a remnant magnetization M_r when the field is switched off. To flip the magnetization in opposite direction a field needs to be applied with strength H_C, called the coercive field.

2.2 Ferromagnetic Resonance

2.2.1 Larmor Precession

Ferromagnetic resonance occurs as a result of the excitation of the precession of the magnetization of a ferromagnet. To understand this, we first look at the behaviour of a single electron spin. The magnetic dipole moment of an electron is proportional to its spin angular momentum S [3].

$$\boldsymbol{\mu} = \gamma \boldsymbol{S}, \tag{2.3}$$

where μ is the magnetic moment and γ is the gyromagnetic ratio ($\sim$ 28 GHz/T). When the electron is in the presence of an external magnetic field $\boldsymbol{B}$, the field exerts a torque on the magnetic moment,

$$\boldsymbol{\tau} = \boldsymbol{\mu} \times \boldsymbol{B} = \gamma \boldsymbol{S} \times \boldsymbol{B}. \tag{2.4}$$

The Hamiltonian of an electron in a static magnetic field $\boldsymbol{B} = B_0 \hat{\mathrm{z}}$ is given by $\mathcal{H} = -\gamma B_0 S_z$. Solving the time-dependent Schrödinger equation and determining the expectation value for $\boldsymbol{S}$ as a function of time t and the angle between $\boldsymbol{B}$ and $\boldsymbol{S}$, α, gives

$$\langle S_x \rangle = \frac{\hbar}{2} \sin(\alpha) \cos(\gamma B_0 t), \quad \langle S_y \rangle = -\frac{\hbar}{2} \sin(\alpha) \sin(\gamma B_0 t), \quad \langle S_z \rangle = \frac{\hbar}{2} \cos(\alpha). \tag{2.5}$$

Thus, $\langle S \rangle$ precesses around the z-axis, under an angle α, with frequency $\omega = \gamma B_0$, as is shown in figure 2.2. This behavior is the Larmor precession of the magnetic moment and the precession frequency is called the Larmor frequency. It increases under the influence of stronger magnetic

fields and for field strengths in the order of 100 mT (typical fields in FMR), the Larmor frequency is in the GHz range.

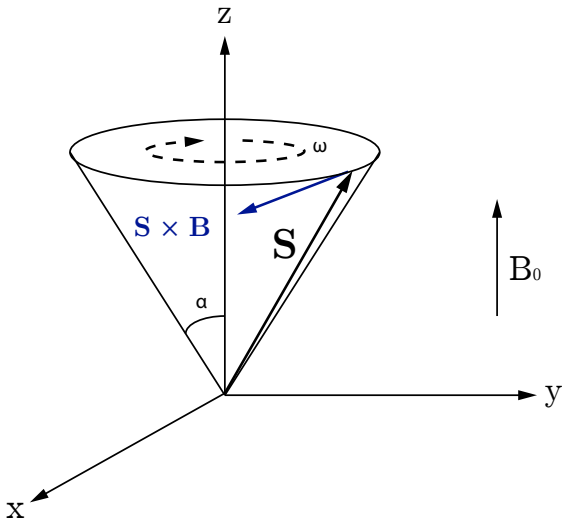

Figure 2.2: Larmor precession of the spin angular momentum of an electron in the presence of a magnetic field B_0.

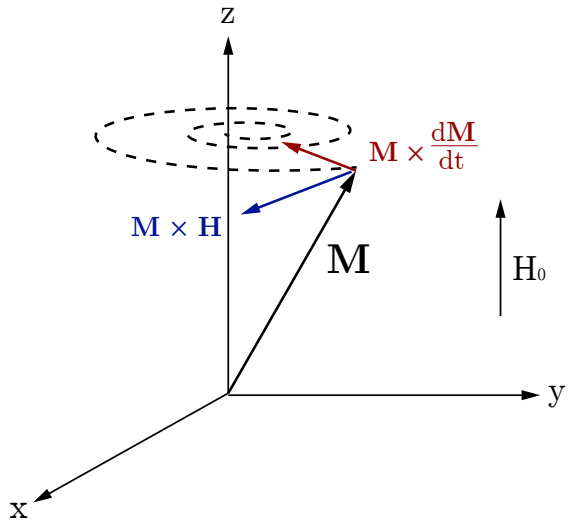

Figure 2.3: Gilbert damping of the precession of the magnetic moment, causing relaxation towards equilibrium.

2.2.2 LLG-equation

To describe the dynamics of the magnetization, M, in a bulk material, all individual spins can be treated as one large macrospin. The magnetization dynamics are described by the Landau-Lifshitz-Gilbert (LLG) equation,

$$\frac{\mathrm{d}\boldsymbol{M}}{\mathrm{d}t} = -\gamma\mu_0 \left(\boldsymbol{M} \times \boldsymbol{H}\right) + \frac{\alpha}{M_S}\left(\boldsymbol{M} \times \frac{\mathrm{d}\boldsymbol{M}}{\mathrm{d}t}\right), \tag{2.6}$$

where H is the magnetic field, μ_0 the vacuum permeability, α the Gilbert damping parameter and M_S the saturation magnetization. The LLG-equation is essentially the torque equation for the Larmor precession (2.4), but with an added term for damping. The first term on the right of the equation describes the precession of the magnetic moment around the magnetic field axis and the second term describes the damping of this precession towards equilibrium, as is shown in figure 2.3. The Gilbert damping is an important property in spintronics since a low damping allows for easy excitation and switching between different magnetic states, thereby requiring little energy, which is promising for the development of fast and energy efficient spintronic memory devices [2].

2.2.3 Polder susceptibility tensor

The LLG equation can be used to describe the dynamics of the ferromagnetic resonance in a material. Ferromagnetic resonance is based on the response of the magnetic moment in a sample

to two different magnetic fields. The first is a static DC field ($\boldsymbol{H_0} = H_0\hat{\mathrm{y}}$) that saturates the magnetic moment M_S in the direction of the field. A second weaker microwave field, excites the precession of the magnetic moment around the effective direction of the magnetic field. The situation is illustrated in figure 2.4, where a sample is excited by a microwave Oersted field emanating from a waveguide.

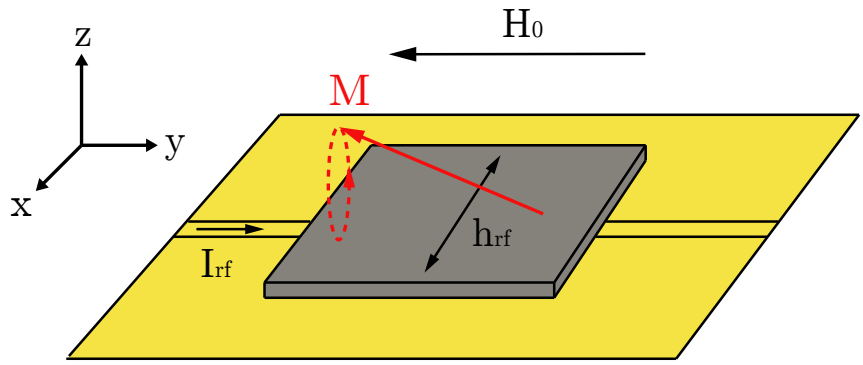

Figure 2.4: The microwave current running through the waveguide induces a microwave field in the sample, exciting the Larmor precession.

The response of the magnetic moment to this excitation is determined by the magnetic susceptibility, χ, which can be found by solving the LLG-equation (2.6) for this problem.

The magnetic moment has a saturated component, M_S, in the y-direction and small time harmonic components $m_{x,z} \sim e^{i\omega t}$ as a result of the precessional motion due to the microwave field. It is assumed that $m_{x,z} \ll M_S$, which gives,

$$\boldsymbol{M} = m_x\hat{\mathrm{x}} + M_S\hat{\mathrm{y}} + m_z\hat{\mathrm{z}}. \tag{2.7}$$

The effective magnetic field depends on four different components. There are two external contributions, namely the external DC magnetic field $\boldsymbol{H_0} = H_0\hat{\mathrm{y}}$ and the RF field $\boldsymbol{h(t)} = h_x\hat{\mathrm{x}} + h_z\hat{\mathrm{z}}$. Next to that the effective field also has two internal contributions. As a result of the magnetic anisotropy there is an out of plane contribution $\boldsymbol{h_k} = \dfrac{H_k}{M_S} m_z\ \hat{\mathrm{z}}$ [4] and last there is a contribution of the demagnetizing field $\boldsymbol{h_d} = -m_z\hat{\mathrm{z}}$ [5], that minimizes the dipole magnetic moment in the film. Combined they give an effective magnetic field

$$\boldsymbol{H_{\mathrm{eff}}} = \boldsymbol{H_0} + \boldsymbol{h(t)} + \boldsymbol{h_k} + \boldsymbol{h_d}. \tag{2.8}$$

Substituting equations 2.7 and 2.8 in the LLG-equation and making a linear approximation by neglecting second order terms and terms of the order $h_{x,y,z}m_{x,y,z}$, gives

$$-i\omega \begin{bmatrix} m_x \\ m_z \end{bmatrix} = -\gamma\mu_0 \begin{bmatrix} M_S h_z + (H_k - M_S - H_0)m_z \\ -M_S h_x + H_0 m_x \end{bmatrix} - \frac{i\omega\alpha}{M_S} \begin{bmatrix} M_S m_z \\ -M_s m_x \end{bmatrix} \tag{2.9}$$

which can be rewritten in the form

$$\boldsymbol{h} = \frac{1}{\gamma\mu_0 M_S}\begin{bmatrix} \gamma\mu_0 H_0 - i\omega\alpha & -i\omega \\ i\omega & \gamma\mu_0(H_0 + M_S - H_k) - i\omega\alpha \end{bmatrix}\boldsymbol{m} \tag{2.10}$$

This equation can be inverted into the form $\boldsymbol{m} = \overline{\overline{\chi}} \cdot \boldsymbol{h}$, where χ is the so called Polder susceptibility tensor. As can be seen in figure 2.4, $\boldsymbol{h}$ is in the x-direction, so only the χ_{xx} component is of relevance, which is given by

$$\chi_{xx} = \frac{M_S(H_0 + M_{\text{eff}} - \frac{i\omega\alpha}{\gamma\mu_0})}{H_0(H_0 + M_{\text{eff}}) - \frac{\omega^2}{\gamma^2\mu_0^2} - \frac{i\Delta H}{2}(2H_0 + M_{\text{eff}})}, \tag{2.11}$$

where $\Delta H = \dfrac{2\omega\alpha}{\gamma\mu_0}$ and $M_{\text{eff}} = M_S + H_K$, the effective magnetization. The real and imaginary part of χ_{xx} are plotted in figure 2.5. As can be seen, the imaginary part of the susceptibility has a Lorentzian line shape and the real part an anti-symmetric Lorentzian line shape, centered at the resonance field. The line width of the resonance can be used to extract the damping and the resonance field is a measure for the effective magnetization. How this can be done is described in the next section.

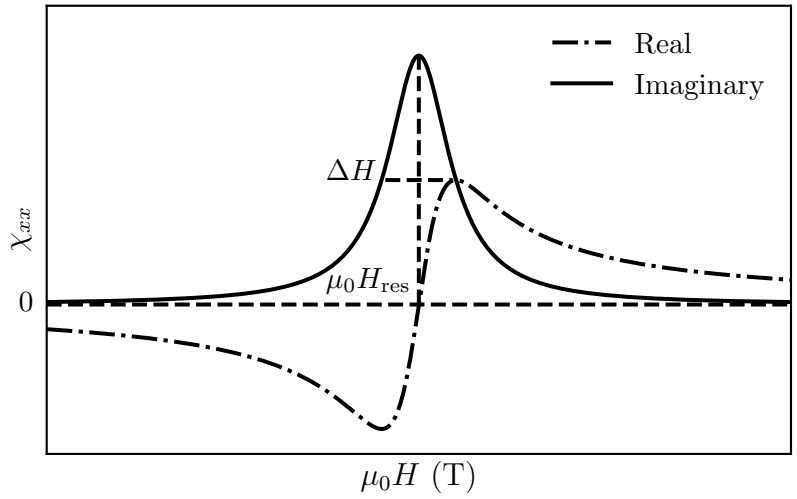

Figure 2.5: Real (dashed line) and imaginary (solid line) part of the Polder susceptibility χ_{xx}. The peaks have a symmetric and anti-symmetric Lorentzian lineshape centered around H_{res} and line width ΔH.

2.2.4 Magnetization and damping

To determine the effective magnetization and damping of the thin film sample, we need to find a relation between the susceptibility, resonance field and linewidth of the absorption peak. The system is in resonance when the absorption peak has its maximum, which is the case when the denominator of the imaginary part of χ_{xx} goes to zero,

$$\left[H_0\left(H_0 + M_{\text{eff}}\right) - \left(\frac{\omega}{\gamma\mu_0}\right)^2\right]^2 + \left[\Delta H\left(H_0 + \frac{1}{2}M_{\text{eff}}^2\right)\right]^2 = 0. \tag{2.12}$$

Assuming $\Delta H^2 \ll H_{\text{res}}^2$, this can be rewritten in the form,

$$f = \left(\frac{\gamma\mu_0}{2\pi}\right)\sqrt{H_{\text{res}}\left(H_{\text{res}} + M_{\text{eff}}\right)}, \tag{2.13}$$

which is known as the Kittel equation. It describes the relation between the resonance frequency, resonance field and effective magnetization and can thus be used to extract the effective magnetization of the sample, by doing a broadband measurement of the resonance peak for different applied frequencies and then fitting the frequency to the resonance field.

The damping in the material can be determined from the line width via [6]

$$\Delta H = \Delta H_0 + \frac{4\pi}{\gamma\mu_0} f\alpha. \tag{2.14}$$

Where the offset ΔH_0 is a correction for inhomogeneous line broadening, due to inhomogeneities in the sample, that lead to multiple resonances around center of the peak. As is clear from equation 2.14, the line width scales linearly with the applied frequency, where the slope is determined by the damping α. By doing a broadband measurement and fitting the linewidth versus the resonance frequency, the damping in the material can be obtained.

Chapter 3

Experimental method

In this chapter we will describe how we can measure the Polder tensor χ_{xx} that was derived in chapter 2. For this, we have assembled a FMR setup that is based on the design developed by Jermain at Cornell University [7]. We discuss the design of the setup and its operation and look at the influence of magnetic field modulation on the measurement of the resonance.

3.1 Setup

As discussed in chapter 2, the damping and effective magnetization rely on the frequency dependence of the linewidth and resonance field. The setup we build was designed to perform broadband FMR measurements, so that we can determine the damping and effective magnetization in a material. Conventional FMR setups use a resonant cavity to excite the precession of the magnetization in a sample. They have one downside however, which is that they can only be used for a measurement at one specific frequency. For a broadband measurement, the resonant cavity has to be replaced, which can be time consuming. To solve this problem, the setup we build utilizes the Oersted field emanating from a broadband waveguide to excite the sample, as is shown in figure 2.4. This allows for a measurement of the resonance for different frequencies without the need to change the resonant cavity each measurement. Since the waveguide only excites a small part of the sample instead of the entire volume, the signal-to-noise ratio (SNR) is significantly reduced. As a solution to this, we apply magnetic field modulation in our setup. This filters out most of the signal that is not field-dependent, thereby improving the SNR.

The waveguide used was designed to have an impedance of 50 Ohms, which is a standard in microwave engineering, since it results in minimal power loss. A sketch of the waveguide is shown in figure 3.1, where the blue lines indicate the power lines through which the microwave current is flowing and the red planes indicate the ground of the waveguide. The transmission of microwave power is dependent on the microwave frequency of the signal.

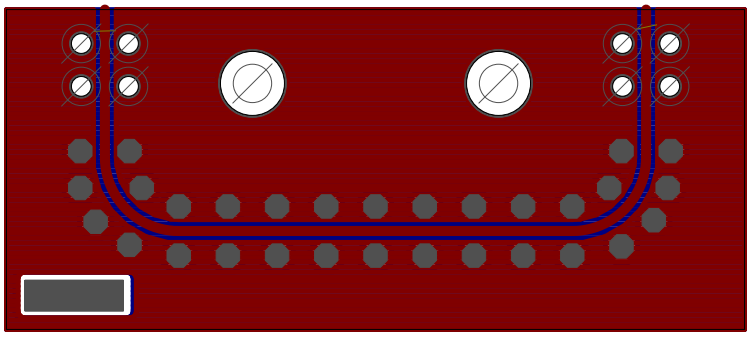

Figure 3.1: Schematic of the waveguide used in the setup.

To investigate the range of our broadband measurements, we determine the power transmission through the waveguide as function of the microwave frequency, which is shown in figure 3.2. As can be seen, the power transmission shows some dips at certain frequencies and shows a general decrease as the frequency is increased. This will result in a smaller signal when measuring the FMR at high resonance frequencies. The loss at the maximum frequency of 20 GHZ is lower than -5 dB however, which should still be sufficient to get a clear signal.

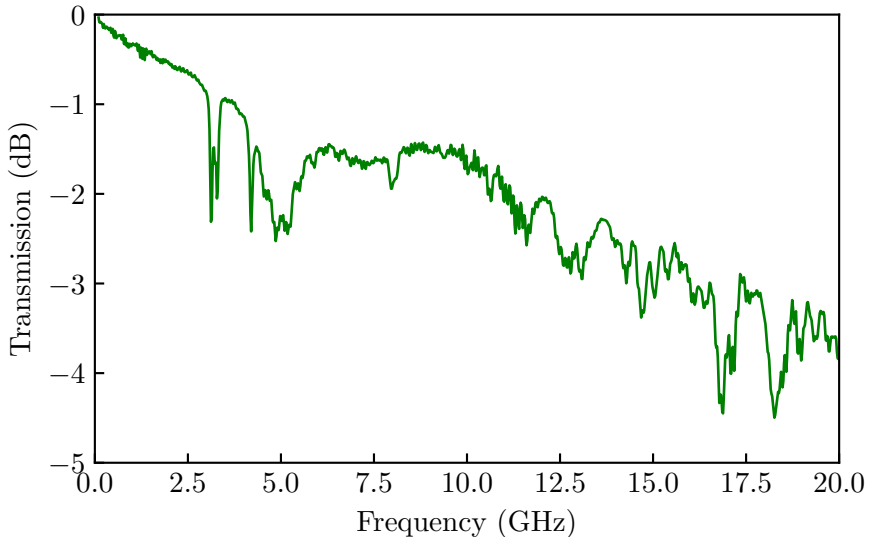

Figure 3.2: Transmission of the microwave power through the waveguide at a microwave power of -10 dBm.

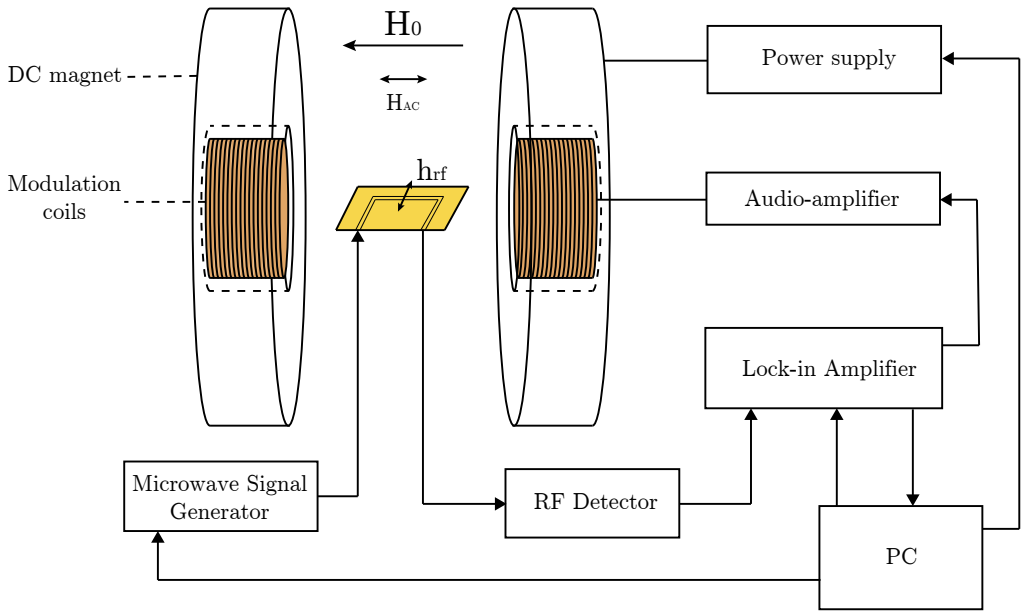

Figure 3.3: Schematic overview of the FMR setup, used in the measurements.

A schematic of the full setup we build and tested is shown in figure 3.3. A waveguide is mounted in between a GMW-3473-70 DC magnet, which has a pole gap of 100 mm and pole face of 150mm. The magnet is powered by a Deltaelektronika SM 70-45 D power supply that supplies a large current to the magnet that induces a strong magnetic field of up to 600 mT (Appendix A.2). An Anritsu MG3692C microwave source generates a microwave signal between 0.1 and 20 GHz at a power of -20 to 30 dBm. It is connected by an SMA cable to the input of the waveguide, where the microwave signal induces a weak microwave magnetic field in the sample perpendicular to the static field. The microwave field excites the precession of the magnetization in the sample, which absorbs the power of the microwave signal. The output of the waveguide is connected by an SMA cable to a Keysight 8474E Diode Detector. In figure 3.4 you see the equivalent circuit of the Diode Detector. A diode polarizes the incoming microwave power which then charges the capacitor. This results in a potential over the capacitor and thus the microwave power is converted to a voltage that can be measured by a Signalrecovery 7265 DSP lock-in amplifier.

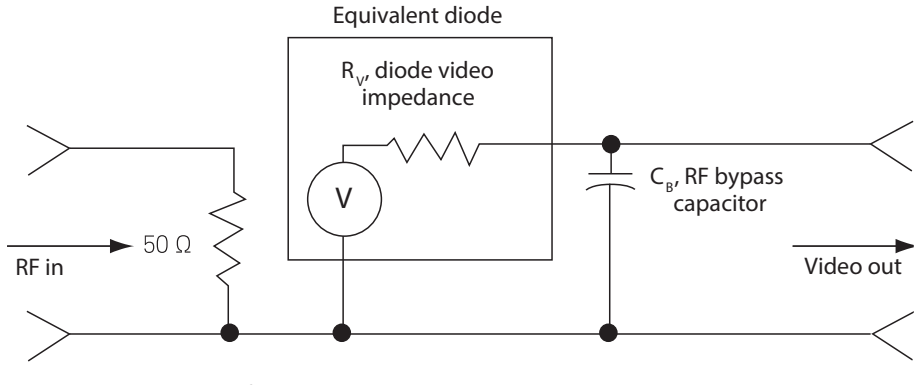

Figure 3.4: Equivalent circuit of the Keysight 8474E Diode Detector.

Field modulation of the magnetic field is applied by two Helmholtz coils, mounted on the poles of the DC magnet. An AC signal that drives the Helmholtz coils is generated by the lock-in amplifier and amplified by an audio amplifier acting as current source. Field modulation in combination with the lock-in amplifier allows us to perform a differential measurement of the ferromagnetic resonance of which the details are discussed in the next two sections.

3.2 Lock-in Amplifier

The output signal of the diode is in the order of millivolts, whereas the the contribution of the resonance in this signal is in the order of microvolts. We need to be able to detect this small signal resulting from the resonance in a larger DC noise. This can be done by using field modulation in combination with a lock-in amplifier, so we first need to understand the operation of the lock-in amplifier.

The lock-in amplifier is an instrument that can detect small periodic signals with a known reference frequency. Say there is a signal

$$V = V_0 \cos(\omega_0 t) + N, \tag{3.1}$$

where N is a combination of various noise components with different frequencies and amplitudes,

$$N = \sum_i V_i \cos(\omega_i t + \phi_i). \tag{3.2}$$

The lock-in amplifier multiplies this signal with a reference signal $\cos(\omega_0 t + \phi)$, giving,

$$V_0 \cos(\omega_0 t)\cos(\omega_0 t + \phi) + \sum_i V_i \cos(\omega_i t)\cos(\omega_0 t + \phi), \tag{3.3}$$

which is then integrated over a time constant τ,

$$V_{out} = \int_t^{t+\tau} \left[V_0 \cos(\omega_0 t)\cos(\omega_0 t + \phi) + \sum_i V_i \cos(\omega_i t)\cos(\omega_0 t + \phi) \right] \mathrm{d}t. \tag{3.4}$$

For $\omega_0 \neq \omega_i$ and provided the time constant is much larger than the period of the signal, the second term goes to zero (based on the orthogonality of cosines). The lock-in amplifier acts as a very narrow band-pass filter around ω_0, that removes nearly all noise of frequencies that are not equal to that of the reference signal. For large enough time constants, the first term will go to $V_0 \cos(\phi)/2$ and thus V_{out} is proportional to the amplitude of oscillation. It has a maximum when there is no phase difference between the input and reference signal. To accurately measure the amplitude of the oscillation, the time constant of integration set by the lock-in amplifier needs to be several times larger than the period, T, of the signal. As the time constant increases, the measurement becomes more accurate, but this also means the measurement will take longer to finish, since the lock-in amplifier needs to integrate the signal over a longer time.

3.3 Field Modulation

As described in section 3.1, the lock-in amplifier is used to generate a field modulation of the magnetic field. In figure 3.5 you see an oscillation of the magnetic field, with amplitude H_{AC}, for a fixed static field H_0. When the magnetic field is oscillating, the absorption of microwave power starts to oscillate as well. The resulting signal measured at the output of the diode is an oscillation between the absorption for $H_0 - H_{\mathrm{AC}}$ and $H_0 + H_{\mathrm{AC}}$. This oscillation is shown in figure 3.6 for four different points on the resonance peak of figure 3.5.

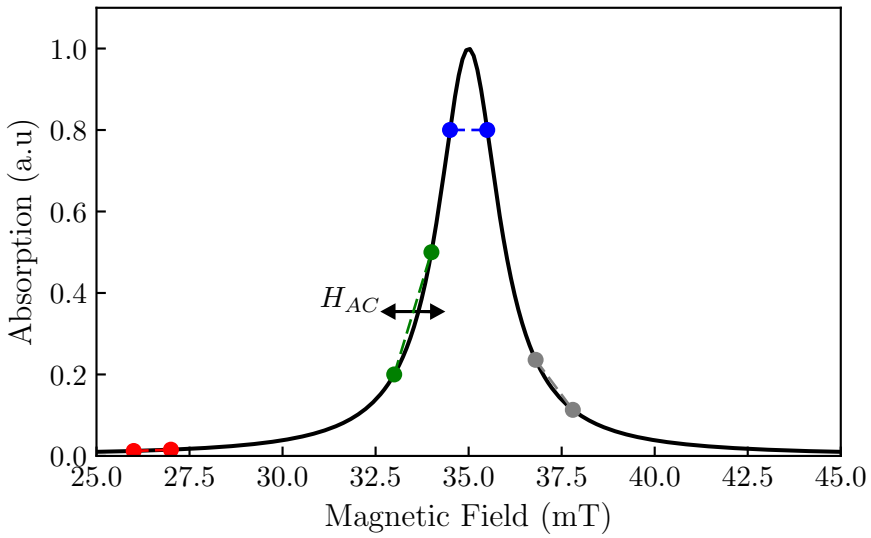

Figure 3.5: Field modulation gives an oscillating magnetic field with amplitude H_{AC} on top of a static field H_0.

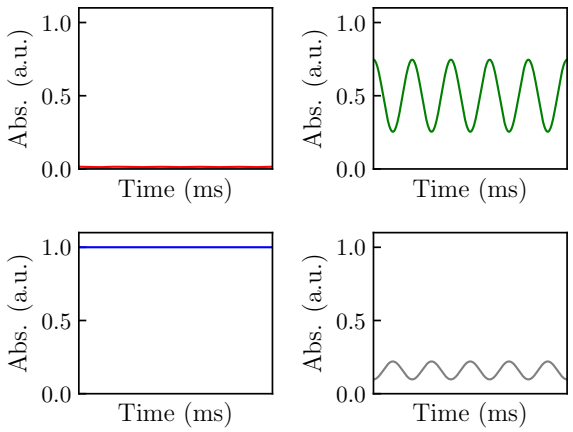

Figure 3.6: Oscillating FMR signal with offset P(H_0) and amplitude $P(H_0+H_{AC})-P(H_0-H_{AC})$.

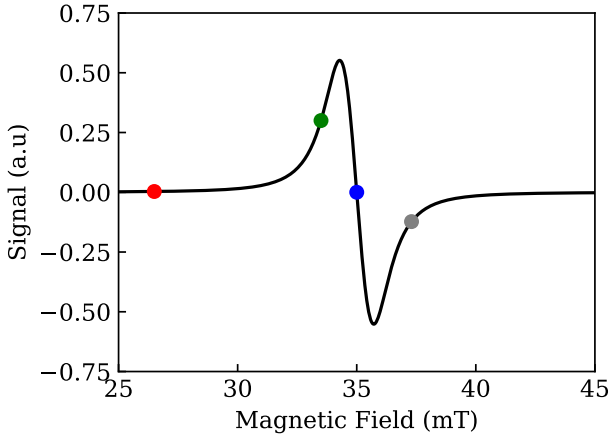

Figure 3.7: Differential spectrum of the FMR signal, as a result of the field modulation.

This oscillating signal in figure 3.6 is measured by the lock-in amplifier that outputs a signal proportional to the amplitude of the oscillation, as discussed in section 3.2. The amplitude is proportional to the derivative of the peak of figure 3.5, so for a sweep of the static magnetic field, this results in a spectrum (figure 3.7) that is the differential of the FMR spectrum in figure 3.5. The differential measurement is used to filter out noise and background from the measurement that is non field dependent, so that the signal-to-noise ratio of the measurement is significantly improved.

When using field modulation, one has to be careful however. When the modulation amplitude of the AC magnetic field is larger than the linewidth of the absorption peak, the measurement signal gets distorted. Because the difference is taken over two points too far apart, the amplitude of the oscillation is not an accurate representation of the slope and the peaks to shift outward. This distortion is negligible when using small modulation amplitudes, but this will result in a decreased signal strength. The behavior of the distortion is illustrated in figure 3.8. For large H_{AC} the signal gets distorted, but for a very small H_{AC}, the oscillation becomes so small that lock-in can barely detect it. When performing the FMR measurement, it should thus be taken into account too not to increase or decrease the modulation amplitude too much, and to find a balance, between signal strength and accuracy.

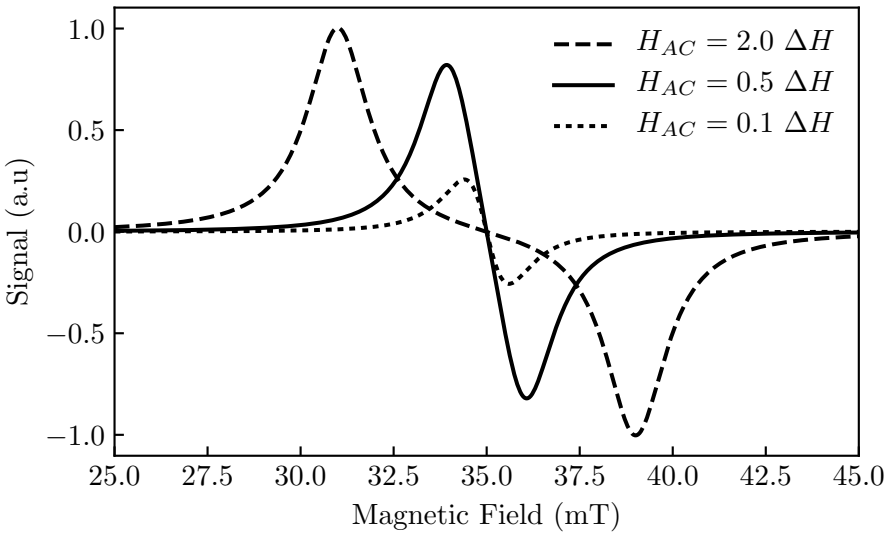

Figure 3.8: Distortion of the differential signal when the modulation amplitude is larger than the linewidth of the FMR peak.

3.4 Measurement

Now that we understand the operation of the setup, we can discuss how a measurement is performed. All equipment is controlled by a PC that runs a software interface for the setup as discussed in appendix A.1. With the interface we set the modulation frequency, modulation amplitude, microwave power and microwave frequency on the lock-in amplifier and signal generator. Then the magnetic field is slowly increased by increasing the current of the power supply that powers the magnet. With each step we measure the power output of the waveguide. The power losses in the waveguide as a result of dissipative processes, are proportional to the imaginary part of the susceptibility (2.10) [9, 10, 11]. Since, we are using field modulation, the measured signal is proportional to the derivative of $\mathrm{Im}(\chi_{xx})$, which has the shape of an anti-symmetric Lorentzian. By repeating this measurement for multiple microwave frequencies, we can perform a broadband FMR measurement. A measurement for each frequency, takes approximately 2-3 minutes, so a full broadband measurement can be performed in under 30 minutes, which is relatively fast and one of the main advantages of this setup.

Chapter 4

Results and discussion

Now that we understand the operation of the setup and know what to expect from a measurement, we can measure the ferromagnetic resonance of the sample. By extracting the damping and effective magnetization of this measurement, we are able to verify the working of the setup. The influence of the modulation amplitude and microwave input power is also discussed.

4.1 Thin film permalloy sample

4.1.1 Measurement

To test the setup and obtain our first results, we measured a sample that is representative for the materials used in research in the Physics of Nanostructures group. We investigate a permalloy ($Ni_{80}Fe_{20}$; Py) thin film sample, with an AlO_x cap to prevent oxidation of the permalloy layer. The permalloy and AlO_x have a thickness of 6 and 2 nm respectively and were deposited on a silicon substrate by sputter deposition. Permalloy is widely used in research involving spintronics, due to its low Gilbert damping.

Unless stated otherwise, we use a modulation frequency of 113.73 Hz, a microwave power of 5 dBm and a modulation amplitude of 0.213 mT (corresponding to 0.3 V on the lock-in output signal) for all following measurements. A single measurement for a resonance frequency of 5 GHz is shown in figure 4.1.

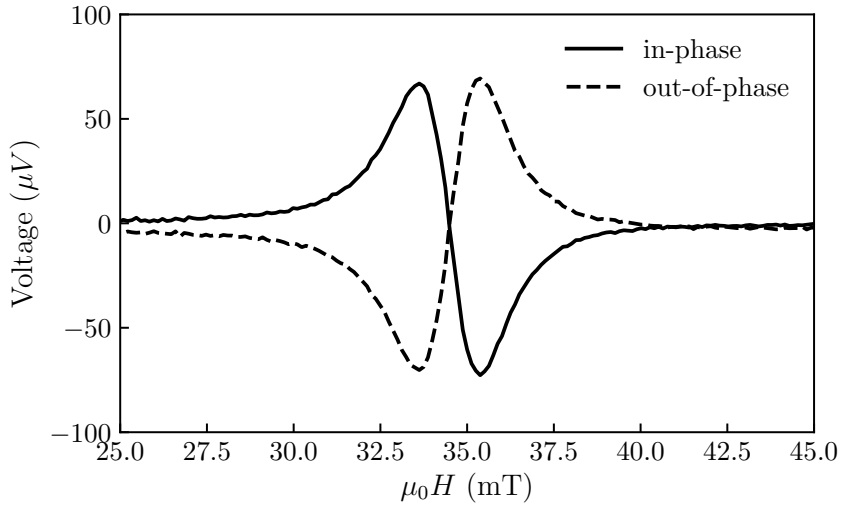

Figure 4.1: In- and out-of-phase component of the FMR signal from a Py sample.

The lock-in amplifier measures both an in-phase (X) and out-of-phase (Y) component with respect to the reference signal. The phase difference of the reference signal can be set manually on the lock-in amplifier to be completely in-phase with the FMR signal, but this changes with different samples and measurement parameters. Using both the in- and out-of-phase components in the analysis can be useful though, since combined they contain more signal of the measurement. Both signals can be combined by using a rotation matrix from coordinate system X and Y to X' and Y', so that most of the signal is in-phase with X' as is shown in figure 4.2.

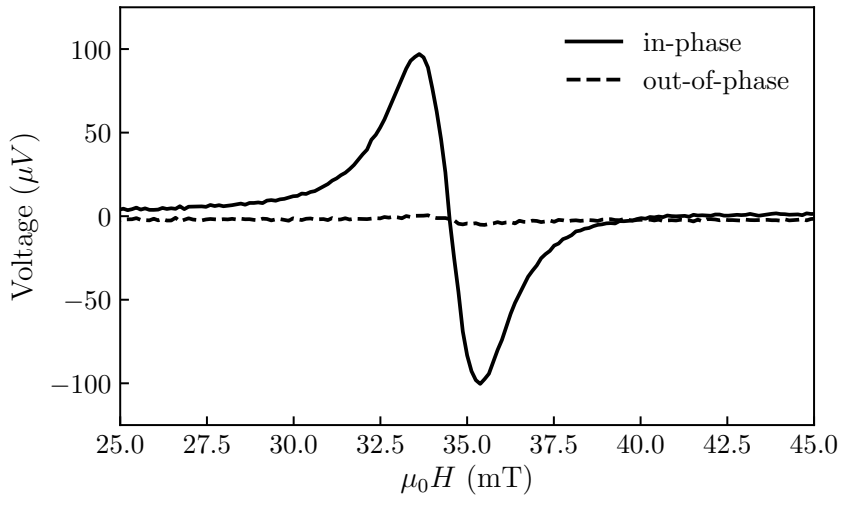

Figure 4.2: After a coordinate transformation, the signal of figure 4.1 is in phase with X'.

This is the type of signal that we expected from section 3.3. To determine the resonant field and linewidth of the peak, the peak is fitted with an anti-symmetric Lorentzian, which has the shape of $\mathrm{Im}(\chi_{xx})$ (eq. 2.10). The fitting equation also includes an offset b and a linear field

dependence c, to account for background noise in the signal.

$$V_{\text{out}} = \frac{A\,(H - H_{\text{res}})}{\left[(H - H_{\text{res}})^2 + (\Delta H/2)^2\right]^2} + bH + c, \tag{4.1}$$

where A is a scaling factor, H the external magnetic field, H_{res} the resonance field, and ΔH the linewidth.

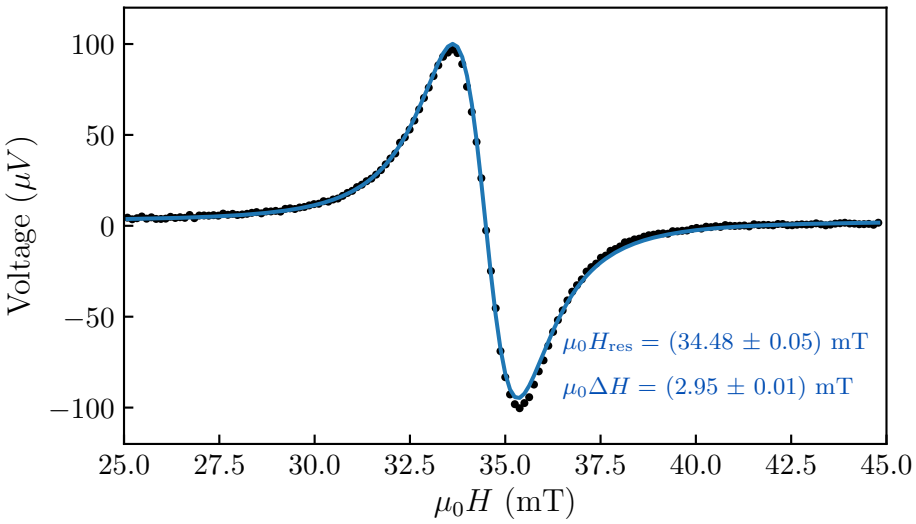

Figure 4.3: Fitting with equation 4.1 determines the value for the resonance field strength H_{res} and linewidth ΔH of the FMR signal.

A fit of the signal is shown in figure 4.3, where we see a slight mismatch at the peaks. This is either background signal or there is a small component of the real part of the susceptibility in the signal. Since this component is small we neglect it from here on.

The same measurement is performed for a range of different resonance frequencies ranging from 2 to 16 GHz, shown in figure 4.4. As can be seen, the resonant field and line width increase with increasing microwave frequency. This behavior is expected looking at equations 2.13 and 2.14. We also see that the signal strength decreases for increasing microwave frequency. The first reason for this is that there is less transmission through the waveguide for higher frequencies, as described in section 3.1. Secondly, the area under each peak should remain constant, so as the width increases the amplitude decreases.

From the relation between the resonance frequency and resonance field and linewidth, the effective magnetization and damping of the material can be determined, which is discussed in the next section.

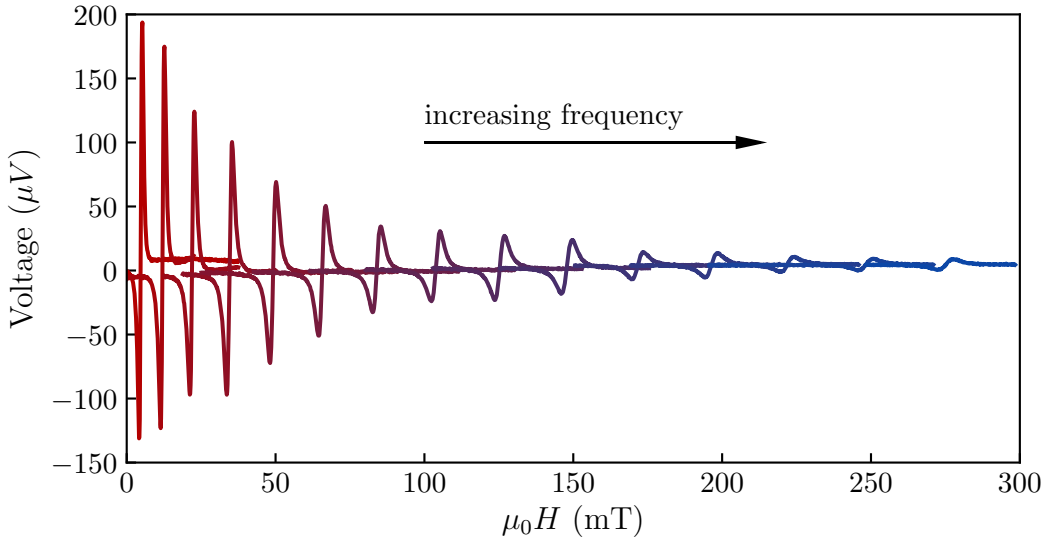

Figure 4.4: FMR spectra for a broadband measurement of a Py (6 nm) sample, ranging from 2 to 16 GHz.

4.1.2 Magnetization and damping

For all frequencies, the resonance field and linewidths are determined by the fitting method described in section 4.1.1. The resonance frequency is plotted versus of the resonance field in figure 4.5 and fitted with the Kittel equation (eq. 2.13). This gives an effective magnetization of the sample of $\mu_0 M_{\text{eff}} = 892 \pm 2$ mT. Literary values for Py layers, with a 5 nm thickness, show an effective magnetization of approximately 0.87 T at room temperature [12], so these results are in good accordance with our setup.

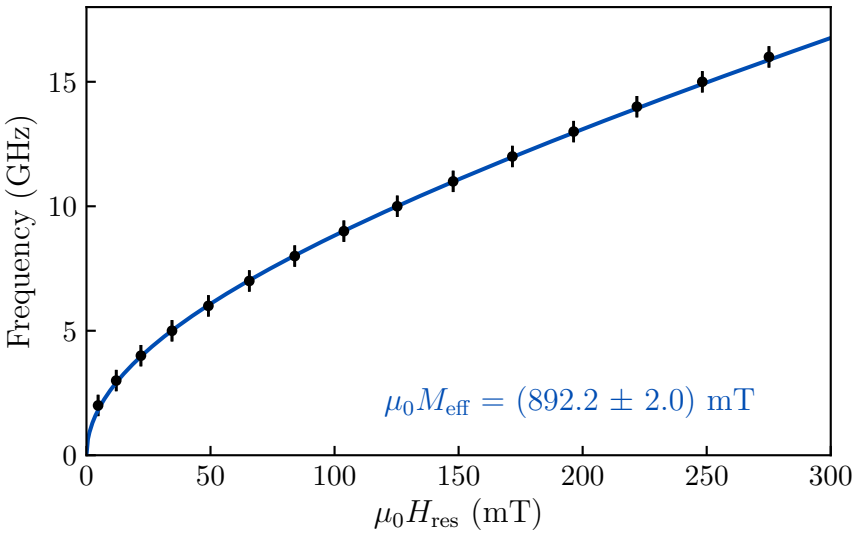

Figure 4.5: A fit of the resonant field strength vs resonance frequency with the Kittel equation (eq. 2.13), gives the effective magnetization in the Py sample.

Next, the linewidths of the resonance peaks are plotted as a function of the resonance frequency in figure 4.6. The slope of the linear dependence between resonance frequency and linewidth is determined by α following from equation 2.14. By fitting this equation we obtain a value for the damping of $\alpha = (7.1 \pm 0.1) \cdot 10^{-3}$. Comparing this value with literature, giving $\alpha = (6.8 \pm 0.1) \cdot 10^{-3}$, our obtained value for the damping is also in good accordance with literature as well.

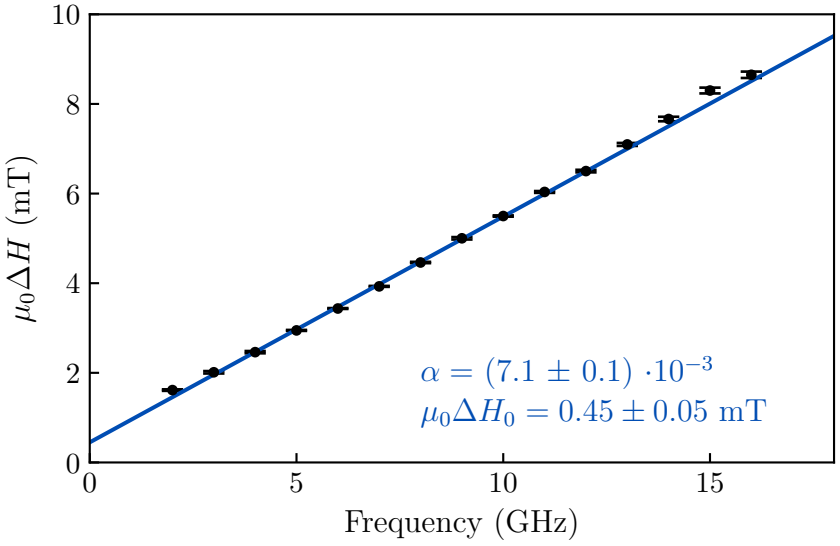

Figure 4.6: A fit of the linewidth of the FMR peak versus resonance frequency determines the damping in the Py sample.

4.2 Measurement parameters

All of the measurements in section 4.1 were performed with the proper measurement parameters, but to determine the limits of the modulation amplitude and microwave power for following experiments, we take a look at how they might distort the FMR signal.

4.2.1 Modulation amplitude influence

To characterize the influence of the modulation amplitude H_{AC} on the signal, as discussed in section 3.3, we perform measurements on the same Py sample with increasing modulation amplitude. The results are given in figure 4.7. The black dashed lines indicate the center of the peaks at low modulation amplitude. As expected from section 3.3, the signal increases in strength with increasing amplitude, but also shows the distortion of the signal, where the peaks shift outward. To relate the lock-in voltage to the AC field amplitude a calibration performed as shown in appendix A.3, which shows $H_{AC} = 0.718$ mT/V for a modulation frequency of 113.73 Hz.

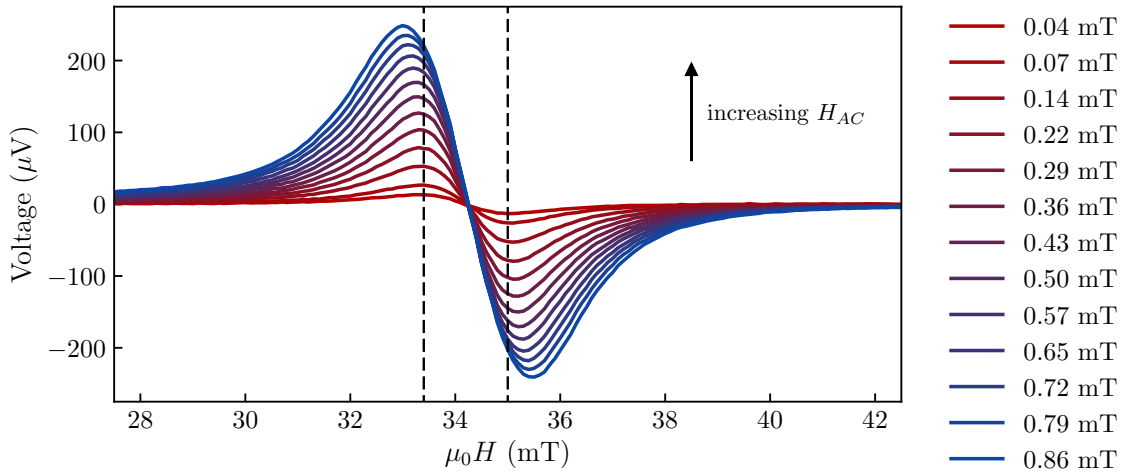

Figure 4.7: Distortion of the FMR signal, shifting the peaks outward, is clearly visible when using higher modulation amplitudes.

Now the linewidth is plotted versus the modulation amplitude in figure 4.8. As can be seen, the distortion of the signal stays within 5% error for $H_{AC} = 0.3$ mT in comparison to the first measurement with $H_{AC} = 0.05$ mT. Increasing the amplitude above that, will distort the signal even more and the accuracy of the measurement will decrease. It is advisable to keep the AC field amplitude below 1/10 of the linewidth, to make sure the measurement is accurate (within 5%). For samples with broad resonances, the modulation amplitude can be increased to obtain a stronger signal, but samples with a very low damping have a very sharp resonance and thus need a small modulation amplitude to perform accurate measurements.

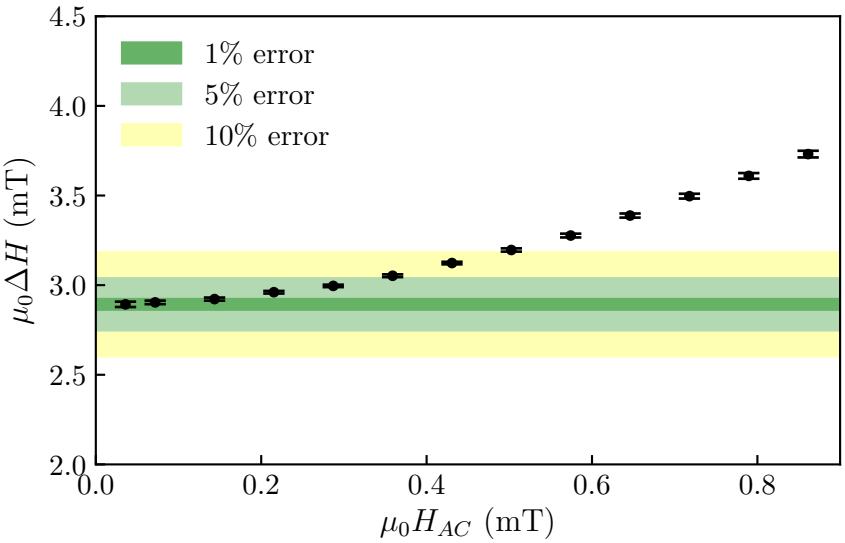

Figure 4.8: Plot of the linewidth versus the AC modulation amplitude.

4.2.2 Microwave power influence

During the derivation of the Polder tensor, we assumed the amplitude of the microwave field was small in comparison to the static field. This linear approximation needs to stay valid in the real scenario as well. We thus investigate the influence of the microwave power on the signal and see if any non-linear effects arise for high powers. The Py sample is measured with increasing microwave power ranging from -10 to 20 dBm, of which the results are shown in figure 4.9. There doesn't seem to be any non-linear behavior at higher powers, so to get a closer look, we normalize the amplitudes of the peaks, so that they overlap (see figure 4.10). Still, the only visible difference, is some noise in the low-power measurements, that does not seem to be caused by any non-linear effects. One note, is that the signal of the 20 dBm measurement, was expected to show non-linear behavior, since this amount of power will likely induce a stronger magnetic field. This could indicate that the power transmission through the cables and waveguide is not sufficient for high power signals and thus the non-linear effects do not occur, but this needs further investigation. Looking at these results, there is no indication that using a high power microwave signal for the excitation is going to distort the measurements. However, the use of a high power microwave signal does significantly increase the background noise and resonances in the measurement as discussed in appendix A.4. When measuring lower quality samples, that do not show strong resonances, this needs to be taken into account, as to not mistake a background resonance as a resonance in your sample.

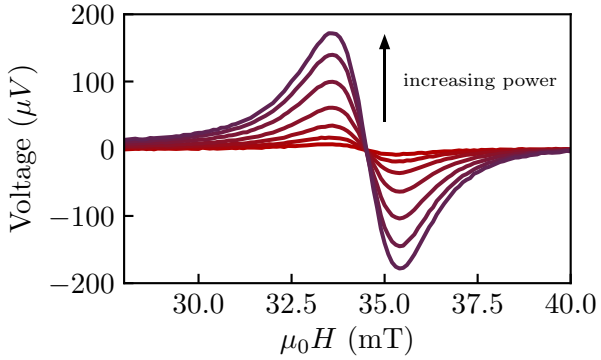

Figure 4.9: FMR spectra for increasing microwave power, ranging from -10 to 20 dBm.

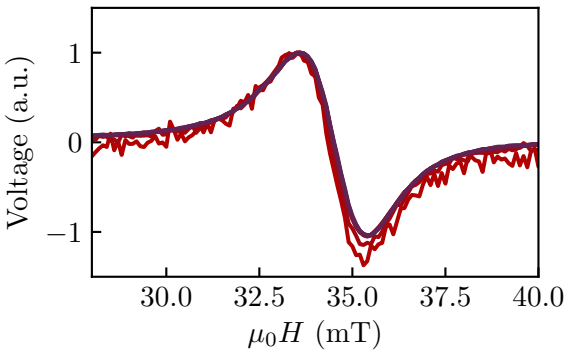

Figure 4.10: Normalized spectra for the measurements in figure 4.9.

Chapter 5

Conclusion

In conclusion, we have discussed the underlying physics needed to understand ferromagnetic resonance and have assembled and demonstrated a fast and accurate measurement setup for the characterization of the effective magnetization and damping in ferromagnetic materials. It can speed up and simplify characterization of the magnetic properties in ferromagnetic materials, which can aid in the characterization and development of new materials that are interesting for research done by the FNA group.
Although the setup shows good results for good to medium quality samples, measurements on a low quality sample (not shown in this thesis) gave lesser results due to background signals. With the subtraction of the background, there was still a measurable response, although this would decrease the usability, that the setup was designed to have. In the next section we outline some improvements that can be made to the setup.

5.1 Setup improvements

When measuring we observe an offset in the background signal of the lock-in (see figure A.4). This background is the result of noise due to the susceptibility of the SMA cables to the AC magnetic field and increases with the strength of the AC field [7] and microwave power. To reduce this noise, amplitude modulation of the microwave power can be implemented in the setup in tandem with the field modulation. Also the use of non-magnetic SMA cables will lead to a reduction of this offset.

Secondly, there is a resonance peak visible in the background signal. This is likely a result of a thin nickel coating, which is ferromagnetic, that the manufacturer used on the waveguide, which is ferromagnetic and thus might cause a background resonance. There is also solder on the waveguide that was used to correct a fault in the design of the waveguide and to solder the SMA connectors to the waveguide. The solder could also be a source for a weak resonance, if

it contains small amounts of ferromagnetic materials. Both problems could easily be resolved by fixing the fault in the design and by replacing the waveguide with one without the nickel coating. It will be more expensive, but can easily be done when there is need for it.

The DC magnetic field induced by the magnets, shows some nonlinear behavior at high currents. This is normal for electromagnets, but it requires more calibration parameters when using stronger fields. There is also a small remnant magnetic field present of approximately 1 mT after the current is turned off as a result of hysteresis. This means that the field determined by the calibration is not one hundred percent accurate, since it depends on the field history. To remove this inaccuracy, a magnetic field sensor can be mounted onto the setup that measures the actual magnetic field during the sweep.

All in all the setup has shown some promising results and has shown to be capable of performing fast and accurate characterization of the magnetic properties of ferromagnetic materials, which is essential to the development of spintronic based devices.

Appendix

A.1 Software interface

The setup is controlled by a software interface we implemented based on a freeware Python package called pyMeasure, available on GitHub. It allows for communication between the equipment and the PC to control the measurement and acquire the measurement results. The control interface makes it possible to do a sweep of the magnetic field, setting the lock-in and microwave generator parameters and measure their output as the magnetic field is increased step by step. The advantage of this software is that it is automatically able to schedule multiple measurements with different measurement parameters. By doing one measurement, an estimation of the effective magnetization can be made and set in the software. The software can then automatically approximate at what field strength the resonance will occur and set a window for the field sweep to save time. This allows for a measurement time of approximately 2-3 minutes per microwave frequency. A full broadband measurement can thus be performed in about half an hour.

A.2 DC magnetic field calibration

The DC magnet used is a GMW-3473-70 with a pole gap of 100mm and pole face of 150mm. To calibrate the magnet, the current that flows through the magnet was slowly ramped up while measuring the induced magnetic field at each step. The results of three different calibrations are shown in figure A.1. As expected, the magnetic field increases linearly with the current applied by the power supply. Only at high currents above 35 A, it starts to show some non-linearity. This should be accounted for when measuring resonances at high microwave frequencies (and thus high magnetic fields), because currently the software uses a linear calibration of 12.62 mT/A, which can be adjusted in the software later on. Since the value of the current is also measured during each step, the calibration can also be adjusted after a measurement. A fit with a third order polynomial is shown in figure A.1, of which the calibrations parameters can be used to relate the applied current and magnetic field. The field can be increased by either decreasing the pole gap of the magnet or using a stronger power.

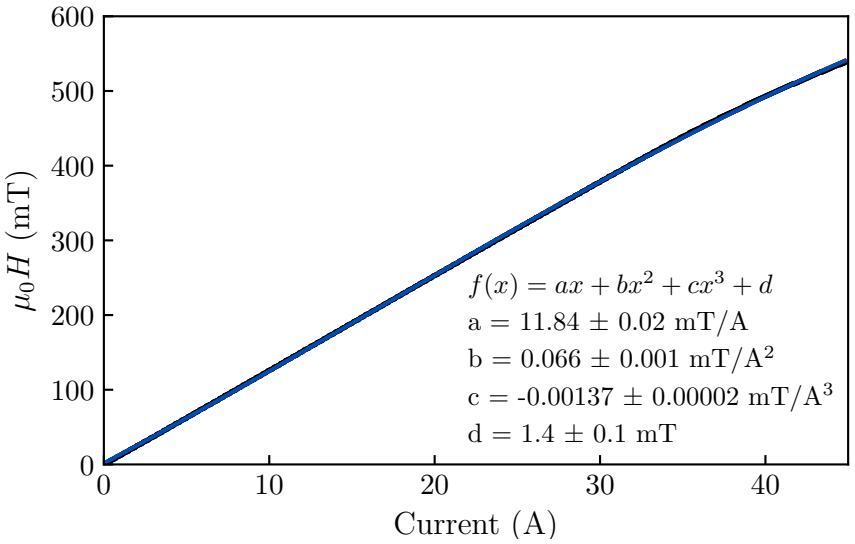

Figure A.1: Calibration of the magnetic field induced by the magnet as function of the applied current, including a fit with a third order polynomial.

A.3 AC magnetic field calibration

The amplitude of the AC magnetic field is determined by the voltage of the external output of the lock-in reference signal. To characterize the amplitude of the AC magnetic field induced by the Helmholtz coils, the voltage of the lock-in signal is slowly increased and AC magnetic field strength is measured for multiple reference frequencies of which the results are shown in figure A.2. The AC magnetic field amplitude shows a linear increase with the applied voltage and a decrease in amplitude when modulating at higher reference frequencies. This is likely the result of an increasing impedance, $i\omega L$, in the Helmholtz coils for higher frequencies. For each reference frequency the slope is plotted in figure A.3. These values are important to take into account when determining the amplitude of the field modulation. As discussed in section 3.3 and 4.1.1 the modulation amplitude needs to stay smaller than the linewidth of the reference peaks as to not distort the signal.

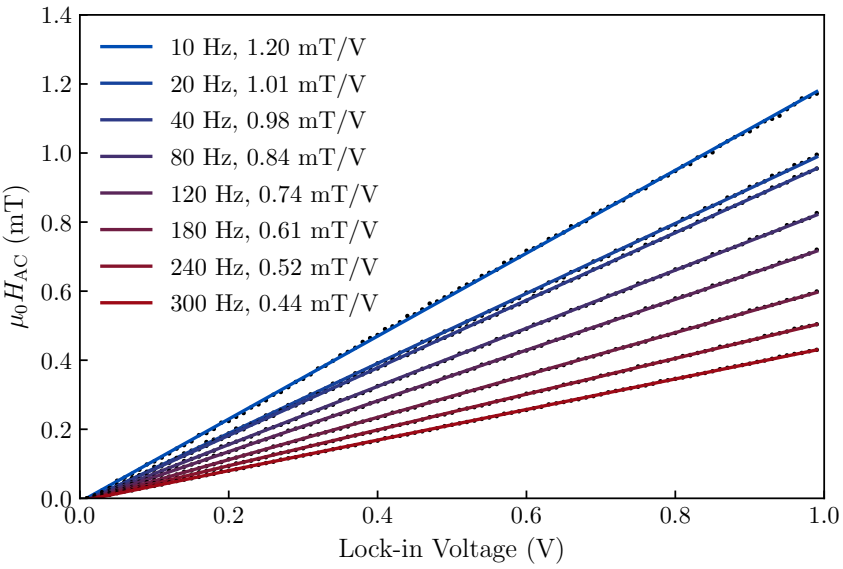

Figure A.2: Calibration of the AC magnetic field as a function of the voltage of the lock-in reference signal for different frequencies.

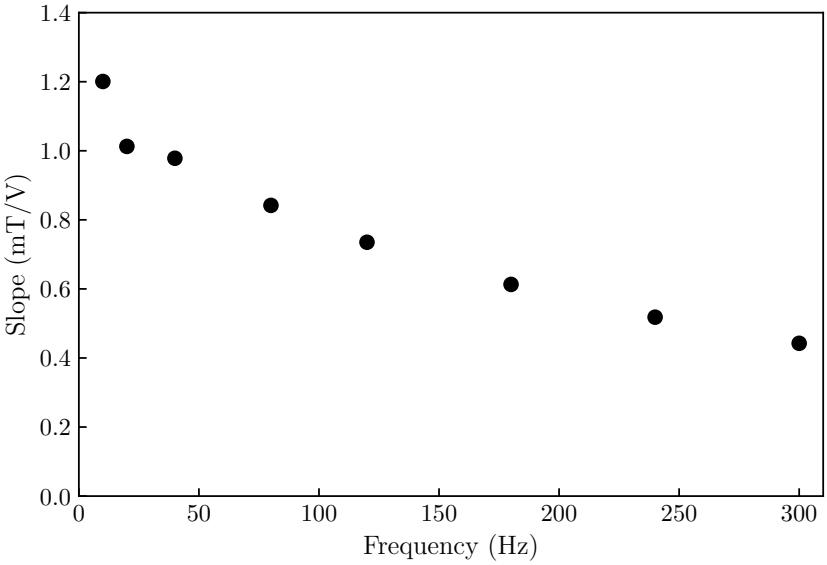

Figure A.3: Slope of the modulation amplitude (mT/V) as a function of the modulation frequency.

A.4 Background signal

When measuring a sample there will be a background present in your signal. This background is a slight offset in the absorption spectrum, mainly caused by the unshielded SMA cables, that are susceptible to the AC field. At high field strengths, there is also significant linear field

dependence visible, as is shown by the red line in figure A.4. The likely reason for this is again the susceptibility of the SMA cables to the magnetic field. When taping the cables down tightly, so they are less mobile, this field dependence was significantly reduced as shown by the blue line in figure A.4. This has already reduced one significant source of background noise.

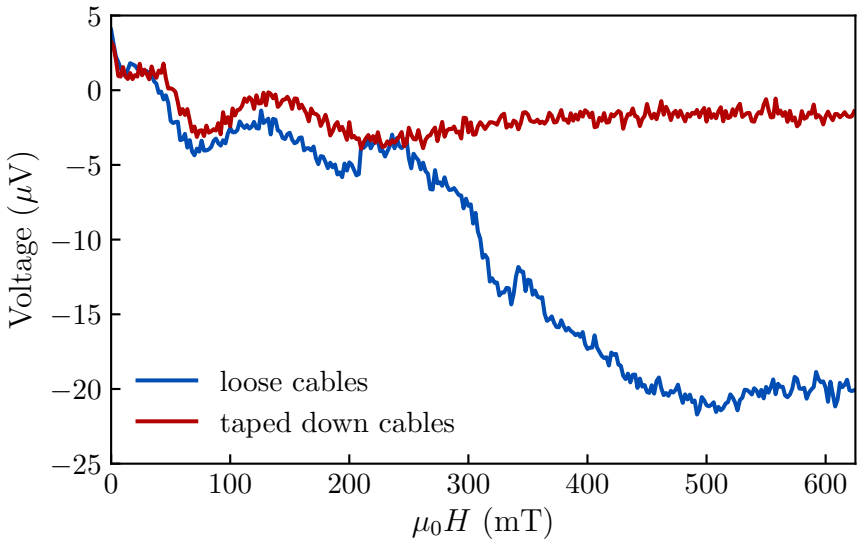

Figure A.4: Background signal, with both loose and taped down cables. Tightly taping down the cables, shows a significant reduction in background noise.

There is also a background resonance visible in the spectrum of figure A.4 around 50 mT. To show that this is not some other noise, one can see in figure A.5 that background resonance is moving as the microwave frequency increases. The most likely source is a nickel coating that the manufacturer used on the waveguide. Nickel is ferromagnetic and can thus be the source of the background resonance. There is also solder present on the waveguide to fix a fault in the design of the waveguide and to attach the SMA connectors onto the waveguide. The solder might contain weakly magnetic materials that may be another possible source for the background resonance. When measuring low quality samples, there is not always a large signal visible from the resonance of your sample, so you need to take into account that the resonance you are seeing might not be coming from your sample.

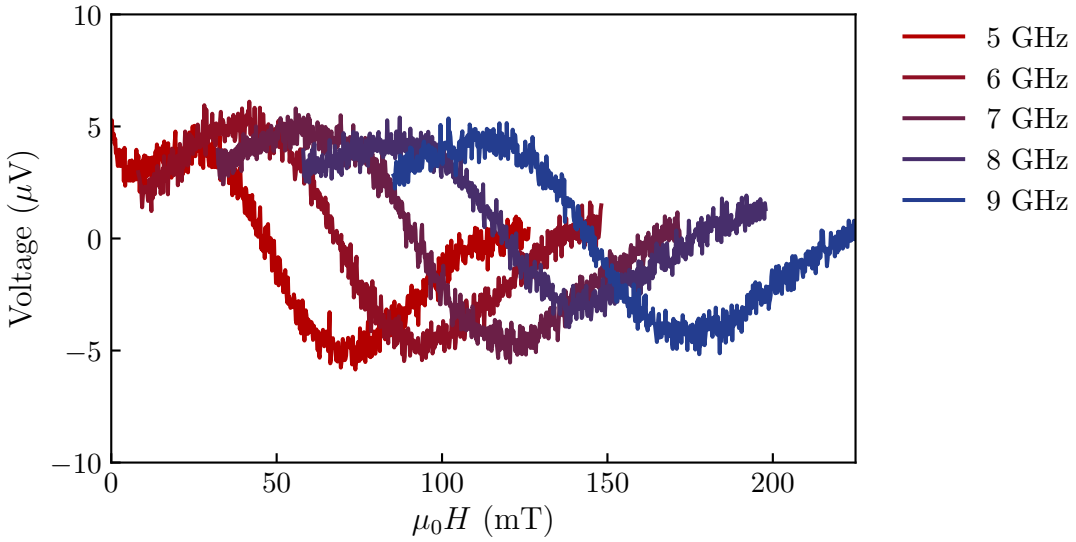

Figure A.5: The resonance background for increasing microwave frequency.

Bibliography

[1] H. Ohno, M.D. Stiles, B. Dieny, *Spintronics*, Proceedings of the IEEE. Institute of Electrical and Electronics Engineers, 104(10), 17821786, 2016.

[2] J.C. Slonczewski, *Current-driven excitation of magnetic multilayers*, Journal of Magnetism and Magnetic Materials, 159-1 pg. L1-7, 1996.

[3] D.J. Griffiths, *Introduction to Quantum Mechanics 2nd Edition*, pg. 180-183, Pearson, 2013.

[4] L. Rutten, *Asymmetric spin wave resonance at Co/Pt interfaces* Technische Universiteit Eindhoven, 2017.

[5] G. Bayreuther, *Magnetic Anisotropy*, University of Regensburg, 2011. Retrieved from http://magnetism.eu/esm/2011/slides/bayreuther-slides.pdf

[6] D.D. Stancil, A. Prahbakar, *Spin Wave Theory and Applications*, Springer, pg. 91-101, 2009.

[7] C. Jermain, *Thesis Chapter 2: Ferromagnetic Resonance Measurement System*, Cornell University, 2017.

[8] Yuelei Zhao, Qi Song, *Experimental Investigation of Temperature-Dependent Gilbert Damping in Permalloy Thin Films*, Beijing, 2016.

[9] M. Balanda, *AC Susceptibility Studies of Phase Transitions and Magnetic Relaxation: Conventional, Molecular and Low-Dimensional Magnets*, Institute of Nuclear Physics, Krakow, 2013.

[10] H. Jiang, C.P. Bean , *Losses in high temperature superconductors as a function of applied field and Frequency*, Rensselaer Polytechnic Institut, Troy, NY, 1995.

[11] M.I. Youssif, A. A. Bahgat, I.A. Ali, *AC Magnetic Susceptibility Technique forthe Characterization of High Temperature Superconductors*, Mansoura University, New Damietta, Egypt, 2000.

[12] Y. Zhao, Q. Song, *Experimental Investigation of Temperature-Dependent Gilbert Damping in Permalloy Thin Films*, Peking University, Beijing, 2015.